





# Biosynthesis and Characterization of Gold and Copper Nanoparticles from *Salvadora persica* Fruit Extracts and Their Biological Properties

Sammar Fathy ELhabal <sup>1</sup>, Hanan Mohamed Elwy<sup>2</sup>, Soha Hassanin <sup>3</sup>, Ahmed A El-Rashedy<sup>4</sup>, Alaaeldin Ahmed Hamza <sup>5</sup>, Mohammad Ahmad Khasawneh <sup>6</sup>

<sup>1</sup>Department of Pharmaceutics and Industrial Pharmacy, Modern University for Technology and Information, Cairo, Egypt; <sup>2</sup>Pharmaceutical Chemistry Department, National Organization for Drug Control and Research, Cairo, Egypt; <sup>3</sup>Biochemistry Department, Modern University for Technology and Information, Cairo, Egypt; <sup>4</sup>Chemistry of Natural and Microbial Products Department, National Research Center (NRC), Giza, Egypt; <sup>5</sup>Biology Department, National Organization for Drug Control and Research, Giza, Egypt; <sup>6</sup>Department of Chemistry, United Arab Emirates University, Al-Ain, United Arab Emirates

Correspondence: Mohammad Ahmad Khasawneh; Alaaeldin Ahmed Hamza, Email [mohammad.khasawneh@uaeu.ac.ae](mailto:mohammad.khasawneh@uaeu.ac.ae); [alaa17mm@gmail.com](mailto:alaa17mm@gmail.com)

**Introduction:** Metal nanoparticle synthesis using plant has emerged as an eco-friendly, clean, and viable strategy alternative to chemical and physical approaches.

**Methods:** The fruit extract of *Salvadora persica* (SP) was utilized as a reducing and stabilizing agent in the synthesis of gold (AuNPs) and copper (CuNPs) nanoparticles.

**Results:** UV–Vis spectra of the AuNPs and CuNPs showed peaks at the wavelengths of 530 nm and 440 nm, respectively. Transmission electron microscopy showed that nanoparticles exhibited a mainly spherical form, with a distribution range of 100 to 113 nm in diameter for AuNPs and of 130 to 135 nm in diameter for CuNPs. While energy-dispersive X-ray spectroscopy was able to confirm the existence of AuNPs and CuNPs. The alcoholic extract of the fruit SP was analyzed by GC-MS in order to identify whether or not it contained any active phytochemicals. Fourier-transform infrared spectra confirmed the presence capping functional biomolecules of SP on the surface of nanoparticles that acts as stabilizers. Analysis of the zeta potential revealed that NPs with high degree of stability, as demonstrated by a strong negative potential value in the range of 25.2 to 28.7 mV. Results showed that both green AuNPs and CuNPs have potential antimicrobial activity against human pathogens such gram-negative bacteria and gram-positive bacteria, with CuNPs having antimicrobial activity higher than AuNPs. In addition, AuNPs and CuNPs have promising antioxidant and anticancer properties when applied to MCF-7 and MDA-MB-231 breast cancer cells. Studies of molecular docking of SP bioactive compounds were conducted against methenyl tetrahydrofolate synthetase. Among all of them, Beta – Sitosterol was the most prominent.

**Conclusion:** These AuNPs and CuNPs are particularly appealing in a variety of applications in the pharmaceutical and medicinal industries due to their economical and environmentally friendly production.

**Keywords:** *Salvadora persica*, green nanoparticles, antioxidant, antibacterial, anticancer

## Introduction

Nanotechnology is a promising multipurpose science used in medicine, pharmaceutical industry, environment, and agriculture. Because of the excellent physicochemical properties of nano-sized particles (such as size distribution, morphology, the surface-to-volume ratio, and surface reactivity-like properties), they found applications in a variety of different fields<sup>1–4</sup>. In general, nanoparticles can be created using chemical or physical processes. Chemical processes lead to the release of harmful substances into the environment, while physical processes require a significant amount of energy and are therefore less economically viable.<sup>2</sup> Therefore, biological fabrication of nanometric materials is the best alternative to overcome the toxicity of chemical methods and the cost of physical methods. In this process, nanoparticles are manufactured using natural, environmentally friendly materials such as plants, bacteria, and algae that are already present in the ecosystem.<sup>2,4–9</sup>

Therefore, biological fabrication of nanometric materials is the best alternative to overcome the toxicity of chemical methods and the cost of physical methods.<sup>5,8</sup> Plant extracts contain biomolecules such as flavonoids, alkaloids, vitamins, terpenoids, alcohols, organic acids, and proteins that are primarily responsible for reducing metals to form nanoparticles. In addition, these compounds serve as capping agents and stabilizers of nanoparticles.<sup>5,7</sup> Extracts of plants belonging to a wide variety of plant species have been employed effectively in the production of numerous metallic nanoparticles, such as copper, gold, silver, iron, and zinc.<sup>7,8,10,11</sup> Because of this diversity, nanoparticles synthesized by this method vary in size distribution, properties and activities, allowing them to function at the level of internal organs.<sup>12</sup> The use of green nanoparticles for copper and gold has garnered more attention than other metallic nanoparticles and has emerged as a distinctive application in the fields of medicine, pharmacy, and biology.<sup>3</sup> This can be explained by the biocompatible nature, facile surface functionalization, and high stability of these materials.<sup>13,21</sup>

The evergreen *Salvadora persica* L. (SP) is a member of the Salvadoraceae family and can be found in the Middle East, Africa, and Asia. It is known by a variety of common names, including miswak, arak, and toothbrush. Its small branches, stems, and roots are utilised in the preparation of chewing sticks due to their effectiveness in maintaining oral hygiene.<sup>14</sup> SP has additional applications, including the treatment of chest ailments, headaches, stomachaches, and ulcers, and is traditionally used for dental care and the treatment of gum infections. Recent research has shown that the SP possesses anti-microbial,<sup>15</sup> anti-oxidant<sup>16</sup> and anti-cancer effect against many types of cancer cells, such as HepG2, MCF7, A549, and HCT116.<sup>16,17</sup> It was discovered that the various portions of SP include essential phytoconstituents such as polyphenols, flavonoids, vitamin C, salvadorine, glycosides, tannins, and saponins.<sup>15,16</sup> Those plant phytochemicals not only participate in the bioreduction of metal ion NPs formation and stability, but also contribute to the bioactivity of the resulting NPs via synergistic therapeutic effects to overcome drug resistance.<sup>3,18</sup> Zinc oxide NPs made from leaves of SP extract have been shown to exhibit toxic against HT-29 cancer cell line.<sup>19</sup> Additionally, silver NPs have been manufactured using aqueous extract of SP roots and were found to have high efficacy of antimicrobial activity against *S epidermidis* and *E. coli* bacteria.<sup>20</sup> More recently, scientific interest in the fruit of SP has increased, as it was found to have an antioxidant, anti-bacterial, and an anti-cancer effects due to the presence of useful active substances such as esters and alkanes, phytosterols, fatty acids, saponins and triterpenoids.<sup>14</sup> In this study, AuNPs and CuNPs were synthesized for the first time utilizing SP fruit extract in an environmentally friendly manner. The comprehensive characterization of green AuNPs and CuNPs utilizing various methodologies, as well as testing them for anti-oxidant, anti-microbial, and anticancer activities.

## Materials and Methods

### Materials

Gold(III) chloride trihydrate ( $\text{HAuCl}_4 \cdot 3\text{H}_2\text{O}$ ) and copper(II) sulfate were purchased from Millipore, Merck. 2-diphenyl-1-picrylhydrazyl (DPPH), 3-(4,5-dimethylthiazol-2-yl) 2,5-diphenyltetrazolium (MTT) viability kit, fetal bovine serum and trypan blue dye were purchased from Sigma (St. Louis, Mo., USA). MCF-7 cells and MDA-MB-231 cells were obtained in liquid nitrogen from the American Type Culture Collection (ATCC, Rockville, MD). RPMI-1640, HEPES buffer solution, L-glutamine, gentamycin and 0.25% Trypsin-EDTA were purchased from Lonza (Belgium). Gram positive (*Streptococcus mutans*, ATCC 25175 and methicillin-resistant *Staphylococcus aureus*) and Gram negative, *Escherichia coli*, ATCC 25922 and *Porphyromonas gingivalis*, EMCC 1699) bacteria strains were obtained from the Regional Center for Mycology and Biotechnology, Al-Azhar University.

### Collection, Authorization and Extraction of the SP Fruit

SP fruits were collected from Al-Muwaiji area in Al-Ain city, United Arab Emirates in May 2021, identified and authenticated by Dr. Nael M. Fawzi. Voucher specimen (14,161) was deposited in the herbarium of the Phyto taxonomy and Horticultural Research Institute, Dokki, Egypt for future reference. The fruit was cleaned and stored in airtight bottles at  $-20^\circ\text{C}$  until the time of extraction. Repeated extractions of a blender-crushed SP fruits were performed in which 50 g samples were macerated with 200 mL of ethanol/water (50/50v/v) at  $4^\circ\text{C}$  for 48 hrs.<sup>21</sup> The extract was then filtered with gauze and centrifuged at 3000 g for 5 min at  $4^\circ\text{C}$ . The resulting supernatant was evaporated in vacuum at

40° using a rotary evaporator to produce a solid residue. A 10% (wt/v) solution of this residue was prepared by dissolving 10 g of this residue in 100 mL of sterile water and kept in a closed container.

## Analysis Using Gas Chromatography-Mass Spectrometry (GC-MS)

The gas chromatograph (7890B) and mass spectrometer detector (5977A) system manufactured by Agilent Technology was utilized in order to determine the active compounds present in the SP fruit extract according to <sup>14</sup>. The Trace GC Ultra-ISQ detector was utilized in order to carry out the trace analysis. Along with a hydrogen carrier gas that had a flow rate of 1.0 mL/min and a split ratio of 10:1, an HP-5MS column that measured 30 m long and had an internal diameter of 0.25 mm was utilized. After the SP extract had been saponified with potassium hydroxide, it was extracted with heptane/diethyl ether, dried, and dissolved in methanol at a ratio of 1:10 by volume. A splitless injection of a 1 microliter sample of this solution was carried out. The temperature of the injection port was set at 280 degree Celsius, and the temperature of the oven was initially set at 70 degree Celsius for five minutes. After that, the temperature of the oven was ramped up to 240 degree Celsius, rising at a rate of 10 degree Celsius per minute to 265 degree Celsius and held for one minute before being increased to 300 degree Celsius at a rate of 15 degree Celsius per minute and being held for 25 minutes. Mass spectra were acquired through the use of electron ionisation (EI) at 70 eV, with a spectral range of m/z 50–550 and a solvent delay of three minutes. Both the bulk and the Quad were at temperatures of 230 degree Celsius. Comparison of the spectrum fragmentation pattern with data held in the Wiley and NIST Mass Spectral Libraries led to the identification of several components of the sample.

## Synthesis of AuNPs and CuNPs Using SP Extract

After dissolving 261 mg of gold precursor in 50 mL of distilled (MilliQ) water, we were able to produce a stock solution of gold(III) chloride trihydrate (HAuCl<sub>4</sub>) that had a concentration of 14.6 mM. (Millipore, Merck). After then, the stock solution was diluted until it had a concentration of 0.1 mM of HAuCl<sub>4</sub>. The synthesis of the gold nanoparticles required the addition of 10 mL of SP extract (10%, weight-per-volume) to a mixture containing 40 mL of 0.1 mM chloroauric acid (HAuCl<sub>4</sub>) solution was stirred while being incubated at room temperature in the dark for twenty-four hours. The hue of the solution changed from a light brown to a dark violet, which is proof that the Au<sup>3+</sup> ions were reduced to Au<sub>0</sub> and that gold NPs were formed. After being rinsed twice with distilled water, the mixture was centrifuged for ten minutes at a speed of 10,000 rpm. For the purpose of analysis, AuNPs pellets were gathered, air dried, and kept at 4 °C.

An aqueous solution of 0.01M copper(II) sulfate (CuSO<sub>4</sub>) was made in distilled (MilliQ) water (Millipore, Merck) (after adding (75 mL) of SP extract (10%, w/v) to 100 mL copper sulfate solution (0.01 M) with stirring at 70 °C. This was done for the Green synthesis of the CuNPs. The color of the mixture has changed from green to orange to reddish brown to brown, which is indicative of the reduction of Cu<sup>2+</sup> ions to Cu<sub>0</sub> and the creation of CuNPs. The color change began when the mixture was green. After 15 hrs, the remedy for the dark brown tint that resulted was established. After being rinsed twice with distillation water, the mixture was centrifuged at a speed of 12,000 rpm for 15 min. After collecting CuNPs pellets, SP-CuNPs pellets were dried at 60 °C for two hrs. and then stored at 4 °C for use in subsequent investigations.

## Physicochemical Characterization of AuNPs and CuNPs

### UV-Vis Spectroscopy Analysis

UV-Vis spectra of the SP extract, AuNPs and CuNPs were recorded using (Jasco, UK model no. V-630) at wavelengths of 200–800 nm. Localized surface plasmon resonance (LSPR) spectra of AuNPs and CuNPs were recorded in quartz crystal cuvettes containing 2 mL of NPs in 1% sodium citrate at a scan speed of 200 nm/min.

### Fourier Transform Infrared Spectroscopy (FT-IR) Analysis

The vibration frequencies of a given compound in FTIR are predicted in a specific region based on both the type of atoms and the type of chemical bonds present in the compound. The FTIR spectrophotometer (Shimadzu 43,000, Kyoto, Japan) was used to describe the chemically possible compound interactions. Briefly, using the KBr disk process, a pure SP-Au-NPs and SP-Cu-NPs

compact disc and its electrospray samples were developed and evaluated at a scan range of 4000–400  $\text{cm}^{-1}$  with a mean spectrum of 32 scans at a 2  $\text{cm}^{-1}$  resolution.<sup>22,23</sup>

## Energy-Dispersive X-Ray (EDX) Spectrometry

To analyze of the elemental composition of the synthesized SP-Au-NPs and SP-Cu-NPs was conducted by using energy-dispersive X-ray (EDX) spectroscopy with JEOL model JSM-IT100 instrument. The results were analyzed based on a set of peaks emitted by a particular element in the electromagnetic emission spectrum.<sup>3,24</sup>

## Transmission Electron Microscopy (TEM) Analysis

For the analysis of external morphology, crystalline nature as well as the size of the synthesized SP-Au-NPs and SP-Cu-NPs, TEM was performed using were analyzed by TEM technique using JEOL (JSM-6510 LV, Tokyo, Japan) electron microscope. For analysis, a drop of the prepared sample was placed on a copper grid and was allowed to dry prior to loading onto the specimen holder. Samples were operated at an acceleration voltage of 200 kV. The grids were then dried under an IR lamp for 50 min before being analyzed.<sup>3,24</sup>

## Measurements of Particle Size and Zeta Potential

Zeta size analysis was used to study particle size distribution, hydrodynamic diameter and zeta potential measurements of NPs using a Zetasizer Nano-Zs90 (Malvern International Ltd, MPT-Z, UK). Zeta potential measurements of NPs are necessary to measure their surface charge, which is related to their stability in solution.<sup>2</sup> The electrophoretic mobility of samples and dynamic light scattering (DLS) is used to measure the dynamic size of the particles in a solution at a scattering angle of 90° at 25 °C. For each sample, the mean diameter  $\pm$  SD for ten runs was calculated by applying a multimodal animation.

## Antioxidant Activity Assay

The antioxidant activity of NPs and ascorbic acid as standard was measured using 2,2-diphenyl-1-picrylhydrazyl (DPPH) method.<sup>25</sup> A volume of 3 mL of 0.004% (w/v) solution of DPPH radical in methanol was added to each tube containing 100  $\mu\text{L}$  of AuNPs or CuNPs (at concentrations of 100, 50, 25, 12.5, 6.25, 3.12, 1.56, 0.78  $\mu\text{g}/\text{mL}$ ). The absorbance was measured at 515 nm after 8 minutes by using a UV–visible spectrophotometer (Milton Roy, Spectronic 1201). Absorbance of the DPPH solution without antioxidants was used as a control, and that of different concentrations of ascorbic acid as a reference standard. The percentage inhibition (PI) of the DPPH radical was calculated according to the formula:  $\text{DPPH-free radical scavenging (\%)} = (\text{Control} - \text{Test} / \text{Control}) \times 100$ .  $\text{EC}_{50}$  value ( $\mu\text{g}/\text{mL}$ ) is the effective concentration at which DPPH radicals are scavenged by 50% and was graphically estimated from graphic plots of the concentration response curve using GraphPad Prism software (San Diego, CA, USA).

## Cell Line and Culture Conditions

MCF-7 cells (human breast cancer) cell line and MDA-MB-231 cells (human breast cancer) cell lines were obtained in liquid nitrogen from the American Type Culture Collection (ATCC, Rockville, MD). Cells were cultured as “monolayer culture” in RPMI-1640 medium with 10% inactivated fetal calf serum and 50  $\mu\text{g}/\text{mL}$  gentamycin at 37 °C inside a humidified incubator with 5%  $\text{CO}_2$  and 95% room air.

## Cytotoxicity Evaluation Using Viability Assay

Using the 3-(4,5-dimethylthiazol-2-yl) 2,5-diphenyltetrazolium (MTT) viability assay, a study was conducted on cancer cells to investigate the cytotoxicity profile of the NPs.<sup>26</sup> At first, the various tumor cells were allowed to remain suspended in media at a concentration of  $5 \times 10^4$  cells per well in Corning® 96-well tissue culture plates for a period of twenty-four hrs. When the cells had been incubated for 24 hours, AuNPs and CuNPs were added to the plates containing them at concentrations ranging from 0.2 to 100  $\text{g}/\text{mL}$ . The plates had 96 wells (three replicates). The MTT test was used to assess, over a period of 24 hours, the total number of viable cells. After removing the medium and replacing it with 100  $\mu\text{L}$  of fresh culture RPMI 1640 media, 10  $\mu\text{L}$  of the 12 mM MTT stock solution (5 mg of MTT in 1 mL of PBS) was

applied to each well. This concludes the removal and replacement of the medium. Following the removal of an 85 L aliquot of the media from each well, 50 L of DMSO was pipetted into each well. The contents of each well were then thoroughly mixed with the pipette before being heated to 37 °C for ten minutes. After that, the optical density was read at 590 nm on the microplate reader (SunRise, manufactured by TECAN, Inc. in the USA), and the result was the number of viable cells. Using the following formula, we were able to determine the relative cell viability in contrast to the group that served as the control:

The formula for calculating the percentage of viable cells is as follows: (A sample minus A blank) / (A control minus A blank) multiplied by 100. The absorbance of a sample is represented by the sample itself. The absorbance of cells after they have been treated with culture medium is an example of a control. The absorbance of the culture media when it is devoid of cells is represented by a blank. GraphPad Prism was used to create visual plots of the dose response curve for each concentration, from which an estimate was made of the concentration known as the 50% inhibitory concentration (IC50), which is the dosage necessary to elicit harmful effects in 50% of intact cells (San Diego, CA. USA).

## Antibacterial Activity of NPs

The antibacterial activity of NPs, plant extract and a standard antibacterial agent were studied against Gram positive (*Streptococcus mutans*, ATCC 25175 and methicillin-resistant *Staphylococcus aureus*) and Gram negative (*Escherichia coli*, ATCC 25922 and *Porphyromonas gingivalis*, EMCC 1699) bacteria. Bacteria strains were obtained from the Regional Center for Mycology and Biotechnology, Al-Azhar University. The well-diffusion assay was applied. About 20 milliliters of nutrient agar medium were poured into the petri plates. Wells for both samples and control made into each agar plate using sterile cork borer. Desired amount of AuNPs, CuNPs and SP extract (100 µg) were loaded on the sterile cork borer (25 mm<sup>2</sup>) in aseptic conditions. Petri plates were incubated for 24 hrs at 37°C. Finally, the average diameter of the inhibition zone surrounding the cork borer was measured using a ruler. The mean and standard deviation (SD) reported for AuNPs, CuNPs and SP extract and with each microbial strain were based on three replicates. Gentamycin (4µg/mL) was used as a positive control.

## Molecular Docking Study

5.10-Methenyltetrahydrofolate Synthetase (MTHFS) regulates carbon flow via the one-carbon metabolic network, which provides crucial components for cell growth and proliferation. MTHFS inhibition has been proven to prevent the growth of human MCF-7 breast cancer cells.<sup>27</sup> Computer-guided docking experiments were carried out using it. The purpose of molecular docking studies was to get deeper insights into the interaction between compounds found in SP extract and 5.10-methenyltetrahydrofolate synthetase receptor. This might lead to a better understanding of the molecular basis of the inhibitory potency and ultimately for lead compound optimization.

## Molecular Docking Study Methodology

The active ligands were produced by adding hydrogens, calculating partial charges, and attempting to minimize energy expenditure with the help of the Force Field MMFF94x. In addition, the creation of proteins involved eliminating the repeating chains, water molecules, and surfactants in order to accomplish the task. The software known as the Molecular Operating Environment (MOE 2015.10, Chemical Computing Group, Montreal, Canada). The capabilities of MOE Quick Prep was utilized in the process of fixing structural faults, calculating partial charges, and protonating three-dimensional models. The MOE Dock protocol's default technique was applied in order to identify the good binding poses of the ligands that were under investigation. The triangle matcher was used as the placement method, and the London dG was used as the primary scoring function. In order to keep poses that had the strongest hydrophobic, ionic, and hydrogen-bond interactions with the protein, an additional refinement step was performed using the stiff receptor approach in conjunction with the GBVI/WSA dG score function. The scores of ligand enzyme complexes were given in kcal/mol in the database that was produced as a result. After that, the results of the docking postures were visually analysed using BIOVIA Discovery Studio, and interactions with the residues of the binding pocket were investigated. The positions that could fit into the binding pocket received the highest ratings and were chosen because they displayed useful ligand enzyme interactions.

## Validation of the Docking Accuracy

The root-mean-square deviation of atomic positions (RMSD) value is usually used to validate the docking protocol, which provides a way to look at crystalline complex protein with a ligand docked inside it. Optimum complex protein has the lowest RMSD value. The docking accuracy of the co-crystallized ligand N-(4-[[[(2R,4S,4aR,6S,8aS)-2-amino-4-hydroxydecahydropteridin-6-yl] methyl(formyl)amino]phenylcarbonyl)-D-glutamic acid (10F) was validated by docking it into the binding site of the human MTHFS receptor. The docking ligand was superimposed on the native co-crystallized ligand with the RMSD of 0.68 Å, and the binding free energy was -15.95 kcal/mol.

## Statistical Analyses

The data obtained were analyzed using the GraphPad Prism programme (version 5) (San Diego, California, USA), and the necessary statistical calculations were made. The growth inhibition zones of bacteria and the cell viability (%) of MCF-7 and MDA-MB-231 were analyzed using a one-way analysis of variance (ANOVA) and Tukey-HSD post-hoc analysis, with  $P < 0.05$  being regarded as statistically significant.

## Results and Discussion

### Phytochemical Analysis of the SP Ethanolic Extract

Major chemical constituents of SP fruit extract estimated by GC-MS are shown in Figure 1 and listed in Table 1 along with their pharmacological activity reported in the literature. Since these phytochemicals are known to have good pharmacological profiles as antioxidant, anticancer and antibacterial agents, we decided to use the SP extract in the synthesis of NPs with aim to study their biological activity.

### Synthesis and Characterization of AuNPs and CuNPs

#### UV-Vis Spectroscopic Analysis

The formation of AuNPs and CuNPs was visually tracked by observing the color change caused by the addition of a metal salt precursor to fruit extract. Color shift of the gold reaction mixture from yellowish green to ruby red indicated

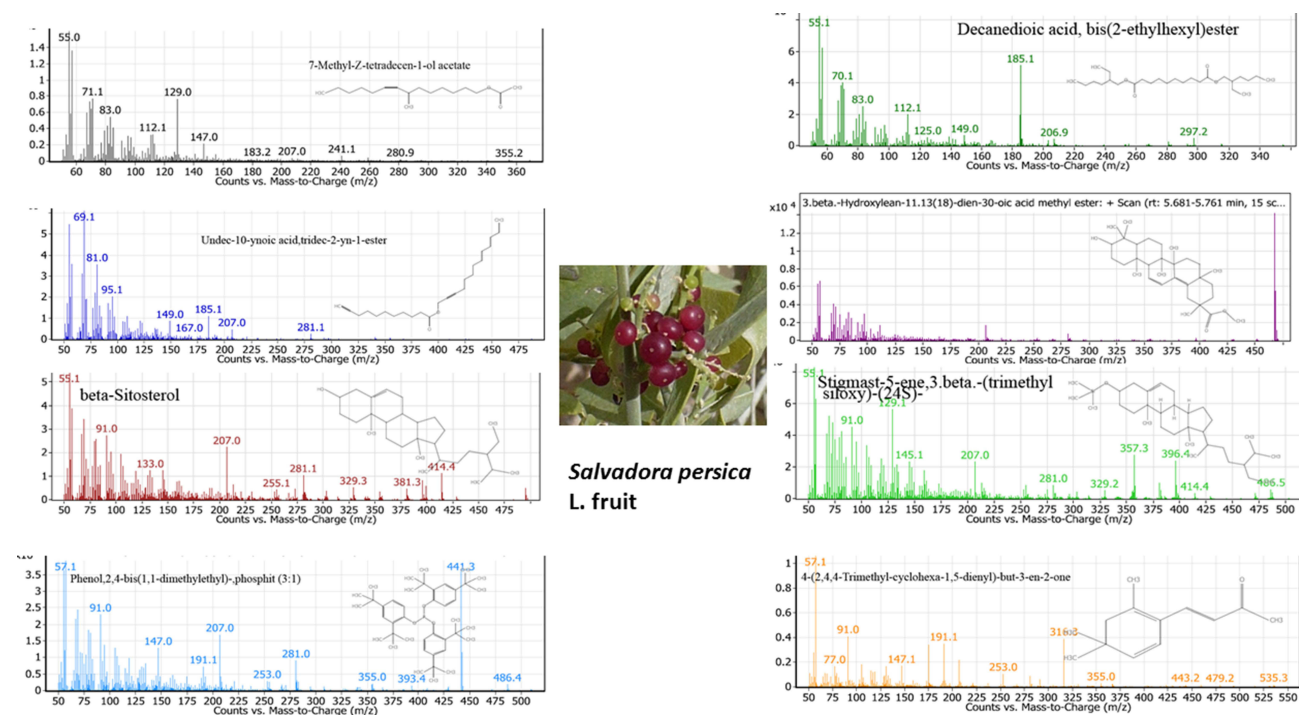


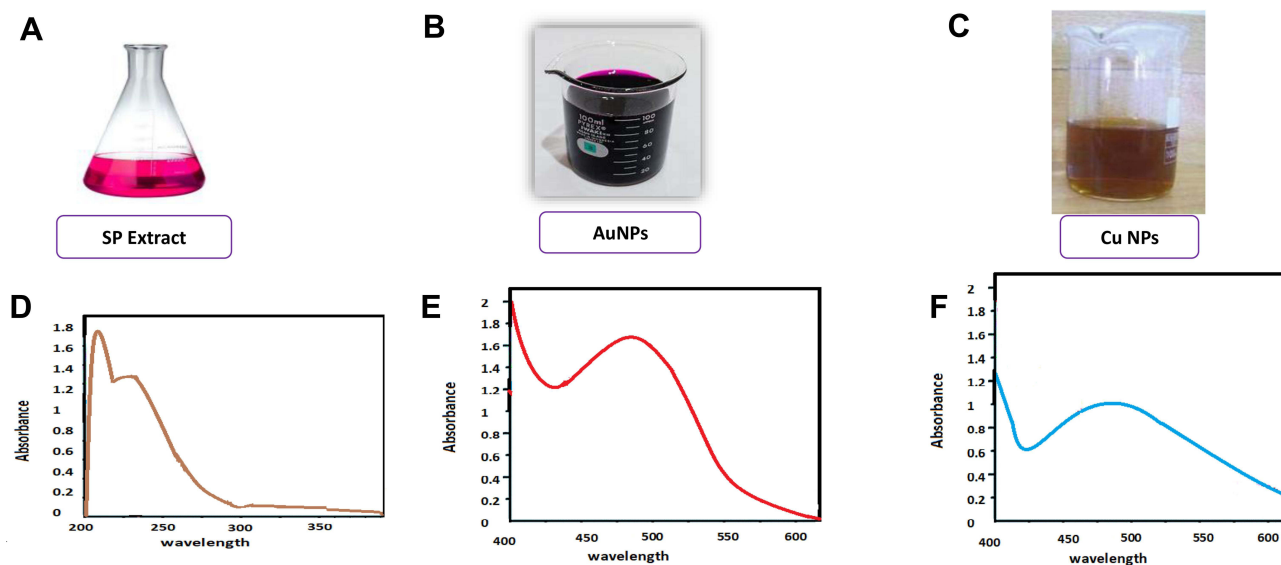
**Figure 1** The main phytochemical compounds identified in the ethanolic extract of SP estimated by GC-MS.

**Table 1** Major Phytochemical Compounds in the Ethanolic Extract of *Salvadora persica* Identified by GC-MS Analysis (Molecular Formulas, Retention Times, Abundance (Area %), and Pharmacological Activity Reported in the Literature)

No	Phytochemical Compound	RT (min)	Formula	Area Sum%	Pharmacological Activity (Ref)
1	7-Methyl-Z-tetradecen-1-ol acetate	2.139	C <sub>17</sub> H <sub>32</sub> O <sub>2</sub>	31.7	Anti-cancer, anti-inflammatory <sup>28</sup>
2	Decanedioic acid, bis(2-ethylhexyl) ester	3.930	C <sub>26</sub> H <sub>50</sub> O <sub>4</sub>	21.33	Antifungal <sup>29</sup>
3	Undec-10-ynoic acid, tridec-2-yn-1-yl ester	4.176	C <sub>24</sub> H <sub>40</sub> O <sub>2</sub>	16.8	Antibacterial <sup>30</sup>
4	3.βeta.-Hydroxylean-11.13(18) -dien-30-oic acid methyl ester	5.681	C <sub>31</sub> H <sub>48</sub> O <sub>3</sub>	21.37	Apoptotic effect, anticancer <sup>31</sup>
5	βeta.-Sitosterol	6.850	C <sub>29</sub> H <sub>50</sub> O	26.4	Anticancer, antioxidant <sup>32</sup>
6	Stigmast-5-ene, 3.βeta.-(trimethylsiloxy)-, (24S)-	7.094	C <sub>32</sub> H <sub>58</sub> OSi	100	Anticancer, antioxidant <sup>32</sup>
7	Phenol, 2,4-bis(1,1-dimethylethyl)-, phosphite (3:1)	7.489	C <sub>42</sub> H <sub>63</sub> O <sub>3</sub> P	19.45	Antioxidant, anticancer <sup>33,34</sup>
8	4-(2,4,4-Trimethyl-cyclohexa-1,5-dienyl)-but-3-en-2-one	8.902	C <sub>13</sub> H <sub>18</sub> O	61.6	Antibacterial <sup>35</sup>

the formation of AuNPs. Similarly, color shift from blue to red-brown in the case of copper reaction mixture indicated the formation of CuNPs. This color shift occurred as a consequence of the NP surface plasmon resonance action due to antioxidant activity of SP. The formation of AuNPs and CuNPs was confirmed visually (Figure 2A–C). UV–Vis spectra of AuNPs and CuNPs are shown in Figure 2D–F. The AuNPs were synthesized using SP extract and an aqueous solution of HAuCl<sub>4</sub>. It was found that the addition of the aqueous extract of SP into HAuCl<sub>4</sub> solution with continuous stirring at room temperature resulted in color change from pale yellow to ruby red color (Figure 2B), indicating the formation of AuNPs. This phenomenon was confirmed by UV–Vis spectroscopy and a sharp surface resonance plasmon (SPR) band was recorded at 520 nm demonstrating the formation of AuNPs (Figure 2E). Similarly, results of absorption peak obtained for AuNPs have been recorded at 523,<sup>36</sup> 530,<sup>37,38</sup> 540<sup>39,40</sup> and 560 nm.<sup>41</sup>

The formation of CuNPs was also confirmed based on the color change of the mixture reaction (Figure 2C), as well as UV–visible spectroscopy (Figure 2F). When the SP fruit extract was added to copper sulfate solution, the color of the solution changed from light blue to red-brown, which confirms the formation of CuNPs. While maximum absorbance peak of CuNPs was obtained at 440 nm. The obtained SPR result was in good agreement with previous results on Cu

**Figure 2** Visual confirmation of SP (A), AuNPs (B), and CuNPs (C) and UV spectra for SP extract (D), AuNPs (E), and CuNPs (F).

plasmonic behavior.<sup>1</sup> Similar results for absorption peak obtained for CuNPs were repeated at 380 nm,<sup>42</sup> 405nm,<sup>43</sup> 540 nm,<sup>44</sup> and 560 nm.<sup>45</sup>

The reaction also involves the reduction of copper metal ions ( $\text{Cu}^{2+}$ ) into CuNPs ( $\text{Cu}^0$ ) with the active substances present in the SP fruit extract, which acts as a reducing agent and also as a stabilizing agent for the reaction. The main functional groups in the plant that participate in the reduction process of metal ions are carbonyl, hydroxyl, amino, amides and methoxy groups, which bind to metal ions by electrostatic interaction, leading to their reduction.

## FT-IR Analysis

FT-IR measurements of the NPs were carried out to identify the major functional groups of phytochemicals present in SP extract. The FT-IR spectra of AuNPs and CuNPs synthesized in the presence of SP fruit extract are shown in Figure 3. Strong bands at  $3442\text{ cm}^{-1}$  and  $3444\text{ cm}^{-1}$  are due to N–H stretching vibration of both amines and amides and/or to O–H stretching vibration of alcohols, phenols or acids. Bands at  $2984$  and  $2890\text{ cm}^{-1}$  are related to C–H stretch of alkanes, whereas bands at  $1643\text{ cm}^{-1}$  and  $1638\text{ cm}^{-1}$  indicate the oxidation of alcohol or carbonyl groups in the presence of gold and copper ions. Bands at  $1466$  and  $1464\text{ cm}^{-1}$  are corresponding to (amine III), where at  $1322\text{ cm}^{-1}$  could be due to C–N stretching or the O–H bending vibrations. The small peaks observed at  $527$ ,  $656$ , and  $537\text{ cm}^{-1}$  are corresponding to metal oxygen vibrations. Similar peaks at  $3094\text{ cm}^{-1}$ ,  $1636\text{ cm}^{-1}$ ,  $1404\text{ cm}^{-1}$ ,  $1322\text{ cm}^{-1}$ , and  $724\text{ cm}^{-1}$  were detected for AuNPs from leaf of SP.<sup>46</sup>

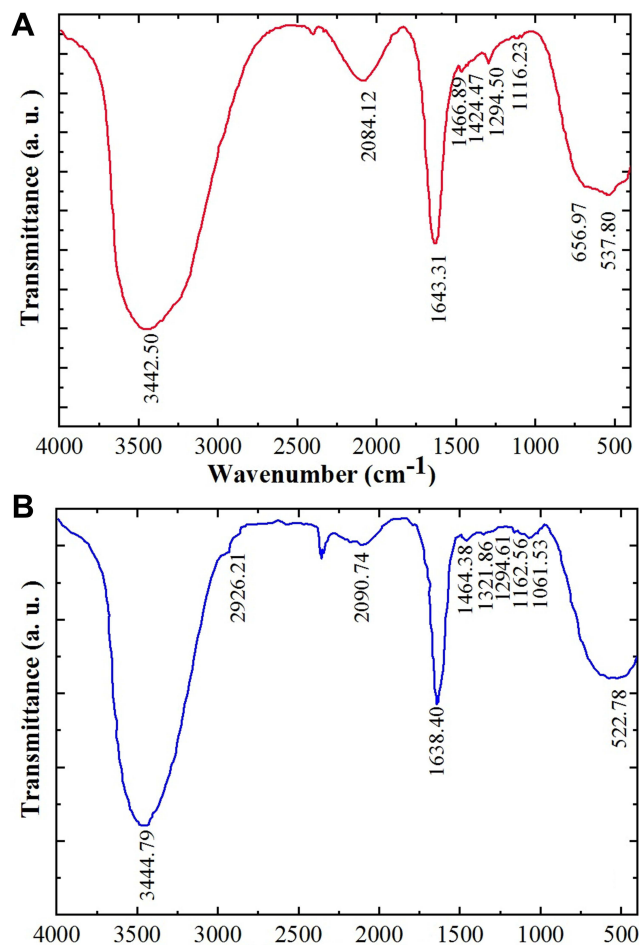


**Figure 3** FT-IR spectrum of both AuNPs (A) and CuNPs (B).



## EDX Analysis

The elemental composition of the NPs was studied by EDX analysis as shown in Figure 4. Figure 4A shows the EDX spectrum of AUNPs, strong signals for gold at different energy levels, mainly at 2.2, 8, 9.8, 11.5 and 12.5 keV, which confirms that the nanoparticles consist mainly of gold. According to the weight percent in Figure 4, the production yield of SP-AuNPs was roughly calculated to be 40%. Weak signals attributed to oxygen and carbon are also observed which is probably related to phytochemicals in the SP extract used to prepare AuNPs. These results are in agreement with previous investigations.<sup>39,47</sup>

Likewise, EDX spectrum of CuNPs (Figure 4B) reveals intense peaks of elemental copper at 1, 2, 3 and 8 keV due to the different energy levels of copper contributing to a weight percent of 44%. This confirms the presence of high copper content in CuNPs.<sup>48</sup> There are also weak signals of oxygen, carbon and calcium, which are substances that may be present in the SP extract and participate in CuNP encapsulation.

## TEM and Particle Size and Zeta Potential Analyses

Properties related to the shape, size and zeta potential of AuNPs and CuNPs in PVP (0.1%) are illustrated in Figures 5 using TEM and zeta size analyses. The primary shape of the particles was spherical with some triangular, hexagons, and rod-like shapes were also observed (Figures 5A and B). Biomolecules, especially flavonoids, alkaloids, terpenoids, nucleic acids and proteins, are able to maintain the directed growth of many shapes during bio mineralization. Most individual AuNPs were uniform and spherical,

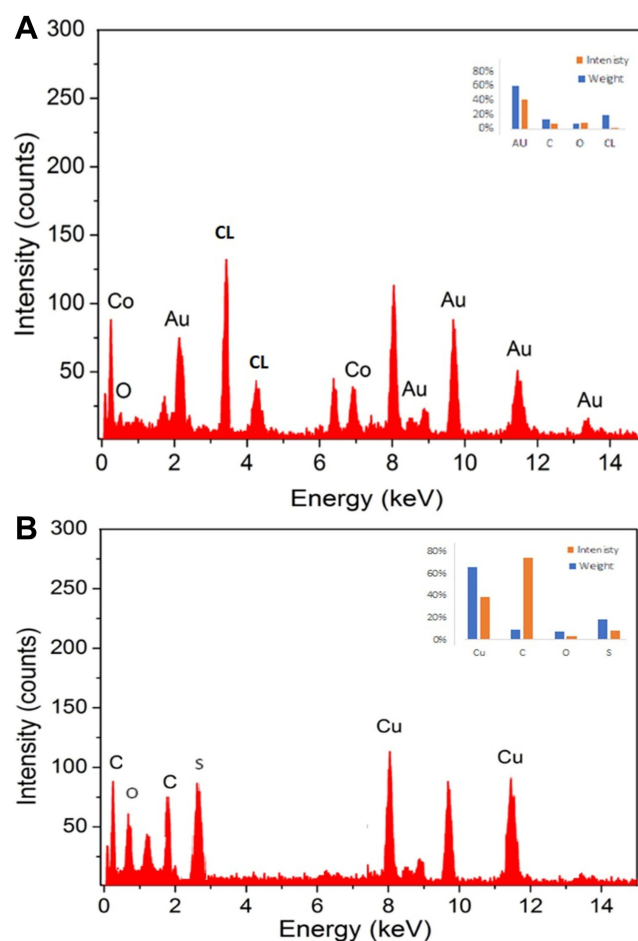


**Figure 4** EDS spectrum for element analysis of both AuNPs (A) and CuNPs (B).

with particle sizes ranging from 100 to 113 nm with an average size of 100 nm (Figure 3A). TEM imaging of CuNPs showed that particles were more spherical when compared to AuNPs with particle sizes ranging from 90 to 139 nm (Figure 5B). The neutral media usually contain mixed salts which may lead to an increase in particle size via sedimentation of aggregates. As a result, the mean hydrodynamic size of NPs was greater than that of Au (Figure 5A and B). Because of the agglomeration experienced by the nanoparticles in DMEM medium, the sizes observed during this study were larger than the sizes determined by TEM. In a previous study, TEM analysis of AuNPs synthesized by *hygrophila spinosa* aqueous extract showed spherical, polygonal, rod and triangular-shaped particles. The authors suggested that various shaped NPs are commonly formed in the same batch during the green synthesis of gold nanoparticles.<sup>39</sup> The particle size of AuNPs by the DLS method was slightly larger compared to that by TEM analysis. The zeta potential of the biosynthesized AuNPs was found to be  $27.78 \pm 0.66$  mV which is similar to our values.

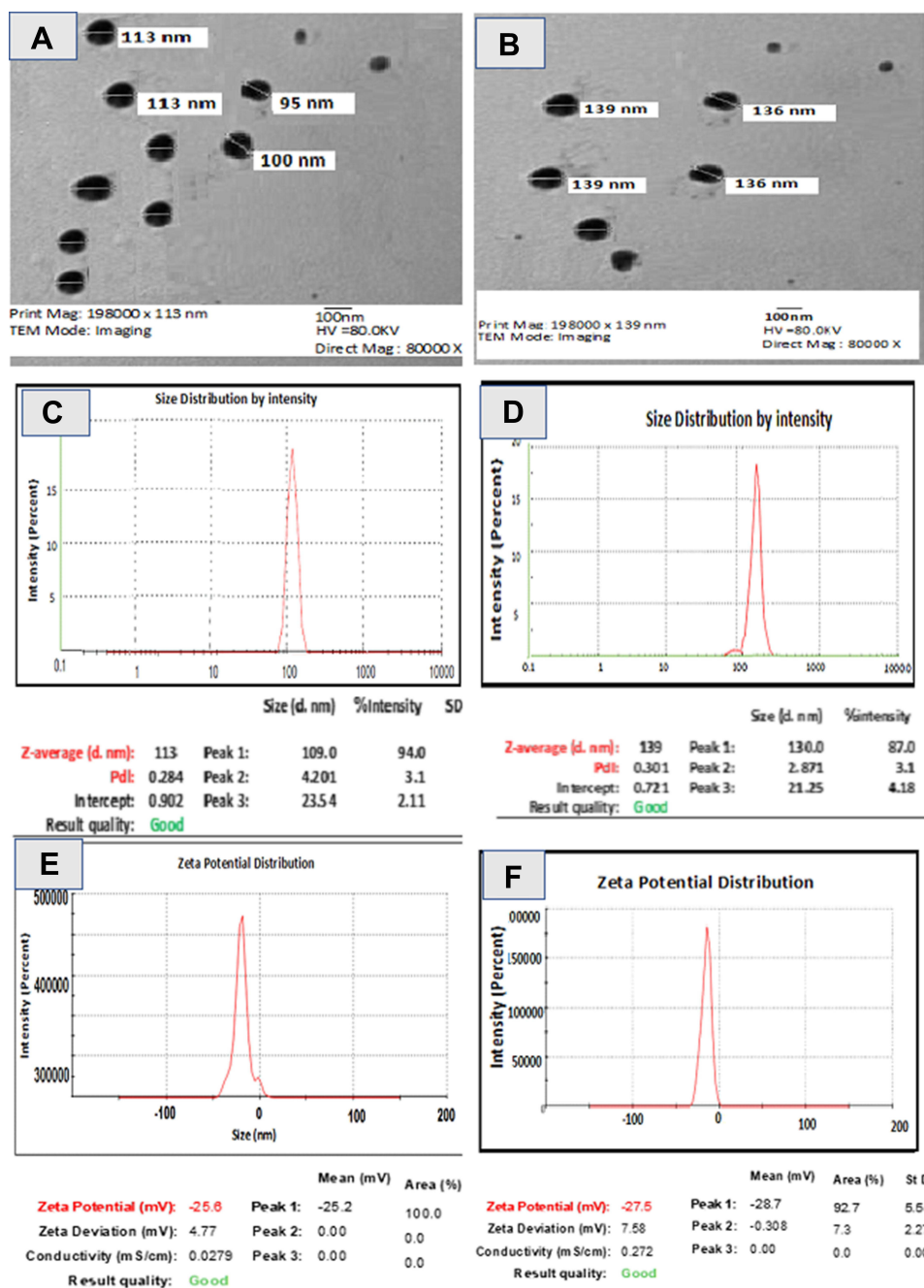


**Figure 5** Determination of size and shape of AuNPs (A) and CuNPs (B) by SEM, determination of size of AuNPs (C) and CuNPs (D) by DLS analysis, and estimation of surface charge of AuNPs (E) and CuNPs (F) by Zeta potential measurement.

This result suggested that the active substances present in the plant extract combined with the surface of the AuNPs and CuNPs stabilized them. In our study, AuNPs had a charge of  $-28.7$  mV, while CuNPs had  $-25.2$  mV (Figure 3E and F). Zeta potential greater than 30 mV or less than  $-30$  mV is indicative of stable dispersions of NPs in solution.<sup>49</sup> These results confirm that the active substances present in the SP extract like sugars, phenolics, flavonoids and proteins, most likely have participated in the negative zeta potential and consequently the stability of the NPs. This negative zeta potential gives repulsive forces in the colloidal solution of PVP-AuNPs endowing its stability and preventing them from aggregations.<sup>3,41</sup>

## Antioxidant Activity of NPs

Free radicals consume the natural defenses of antioxidants in the body, which leads to the oxidation of proteins and fats in the body, leading to oxidative stress that occurs in all degenerative diseases. Therefore, antioxidants found in medicinal plants are needed to maintain good body health.<sup>50</sup> In this study, the antioxidant potential of the green AuNPs and CuNPs was evaluated using DPPH, a stable free radical with a purple color that turns yellow in the presence of antioxidants. The DPPH radical is scavenged by antioxidants through the donation of hydrogen radicals ( $H\cdot$ ) to form the stable DPPH-H molecule.<sup>25</sup> This radical scavenging activities of ascorbic acid, SP extract and nanoparticles were increased with increasing concentration as shown in Figure 6. The  $IC_{50}$  values of AuNPs, CuNPs, ascorbic acid and SP extract were  $5.52 \pm 0.47$ ,  $6.72 \pm 0.67$ ,  $10.64 \pm 0.82$ ,  $15.69 \pm 1.23$   $\mu\text{g}/\text{mL}$ , respectively (Table 2). These results confirm the high antioxidant potential of the NPs compared with ascorbic acid and SP extract and are consistent with what were previous reports.<sup>42,51,52</sup> The antioxidant activity of NPs can be linked to the existence of a number of phytochemicals, which are believed to work in concert and cooperatively to combat free radicals. The outcomes significantly support the use of fruit extracts of SP-mediated AuNPs and CuNPs as helpful natural antioxidants for protecting against various forms of oxidative stress linked to degenerative illnesses.

## Antibacterial Activity of AuNPs and CuNPs

Bacterial infections are often associated with several chronic diseases that may lead to death. Metallic nanoparticles may offer an excellent option for bacterial inhibition due to their diverse mode of action as the nanoparticles combine with the negative charge on the surface of the bacteria cell membranes without penetrating the wall.<sup>3</sup> SP fruit extract and green AuNPs and CuNPs were investigated for their effect against two different gram-negative types (*E. coli* and *P. gingivalis*) and two gram-positive (*S. aureus* and *S. mutans*) bacteria and the results are outlined in Table 3. Metal NPs are believed to combat bacteria through a number of modes of action. They promote pathogenic inactivation either through (1) diffusion, where ROS are introduced into the bacteria through the diffusion process, or (2) biosorption, where the released ions in the environment bind with the negatively charged functional groups like carbonyl and phosphate that are present on the surface of the bacterial cell.<sup>3</sup>

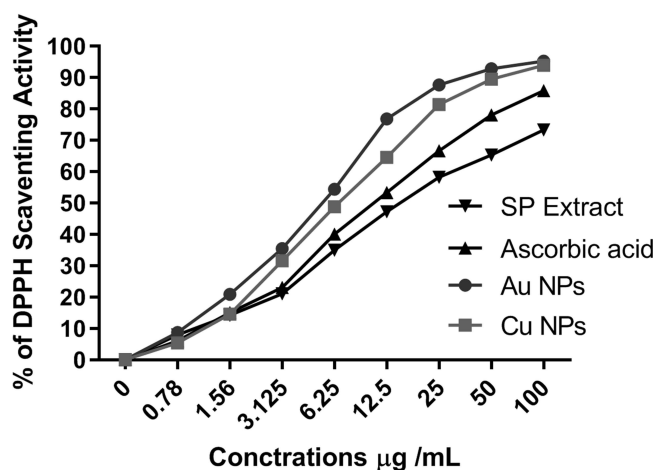


**Figure 6** The antioxidant properties of AuNPs and CuNPs, ascorbic acid and SP extract against DPPH.

**Table 2** The IC<sub>50</sub> of AuNPs, CuNPs, Ascorbic Acid and SP Extract in the DPPH Test

	AuNPs	CuNPs	Ascorbic Acid	SP Extract
IC <sub>50</sub> of DPPH	5.52 ± 0.47 µg	6.72 ± 0.67 µg	10.64 ± 0.82 µg	15.69 ± 1.23 µg

Notes: IC<sub>50</sub> is the concentration of the corresponding NPs that are able to scavenge DPPH radicals by 50%.

**Table 3** The Growth Inhibition Zones of Bacteria in Agar Disk Diffusion Assay in Selected Concentration of AuNPs, CuNPs, SP Extract and Gentamycin

Conc.	Inhibition Zone in Disk Diffusion (mm)			
	Gram-Negative Bacteria		Gram-Positive Bacteria	
100 µg/mL	<i>Escherichia coli</i>	<i>Porphyromonas gingivalis</i>	<i>Streptococcus mutans</i>	<i>Staphylococcus aureus</i>
AuNPs	R	23 ± 0.60 <sup>a</sup>	R	31 ± 1.10 <sup>a</sup>
CuNPs	12 ± 0.44 <sup>b</sup>	15 ± 0.40 <sup>c</sup>	R	27 ± 0.66 <sup>b</sup>
SP Extract	R	R	R	R
Gentamycin	30 ± 0.40 <sup>a</sup>	18 ± 0.40 <sup>b</sup>	22±0.50	15 ± 0.40 <sup>c</sup>

Notes: Values are means ± SD of triplicate experiments. Means in the same column with different letters were significantly different (P<0.05), ANOVA, Tukey-HSD, Control =Gentamycin (4 mg/mL). Means in the same column with different letters were significantly different (P < 0.05).

Abbreviation: R, resistance.

AuNPs showed the highest effect against *Staphylococcus aureus* (31 ± 1.10 mm inhibition zone diameter) and *P. gingivalis* (23 ± 0.60 mm inhibition zone diameter). As shown in Table 3, there was no effect of AuNPs on *E. coli*. A previous report found the highest effect of AuNPs synthesized from Chinese lettuce against *Staphylococcus aureus* (40 mm inhibition zone diameter) with no effect on *E. coli* cell growth.<sup>51</sup> SP extract alone had no effect on preventing the growth of the analyzed bacterial strains. This is consistent with a previous study on SP extract from the fruit where it was ineffective against other gram-positive as well as gram-negative bacteria at a concentration of 100 µg/mL.<sup>14</sup> The highest zone of inhibition observed for CuNPs was against *S. aureus* (27 ± 0.66 mm) followed by *P. gingivalis* (15 ± 0.40 mm), and *E. coli* (12 ± 0.44 mm), respectively. In a previous report where CuNPs were synthesized from ginger extract, they were found to have higher inhibitory effect on *S. aureus* than on *E. coli*. The authors attributed this to the fact that *S. aureus* has little negative accusation compared to *E. coli*.<sup>53</sup> It is interesting to mention that both AuNPs and CuNPs had a higher inhibitory effect on methicillin-resistant *S. aureus* than that of the standard aminoglycoside antibiotic drug used in our study (gentamycin).

## In vitro Anticancer Effect of AuNPs, CuNPs and SP Extract

The anticancer effects of AuNPs, CuNPs and SP extract were quantified with MTT assay against MCF-7 and MDA-MB-231 human cell lines. The cell viability data (Figure 7) were found to be concentration dependent, which confirms their anti-cancer

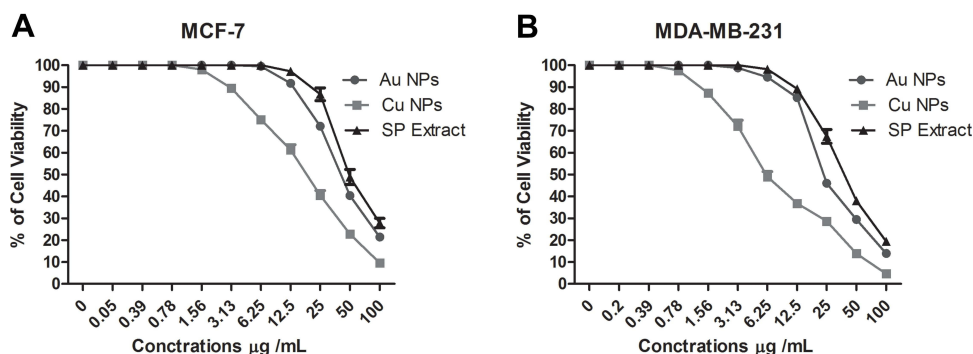


Figure 7 Cell viability (%) of MCF-7 (A) and MDA-MB-231 (B) human cancer cell lines were treated with different doses of AuNPs, CuNPs, and SP extract.

**Table 4** IC<sub>50</sub> for MCF-7 and MDA-MB-231 in Selected Concentrations of AuNPs, CuNPs, SP Extract

	IC <sub>50</sub> for MCF-7	IC <sub>50</sub> for MDA-MB-231
<b>AuNPs</b>	42.41 ± 2.63 µg/mL <sup>a</sup>	23.73 ± 1.75 µg/mL <sup>a</sup>
<b>CuNPs</b>	19.34 ± 1.68 µg/mL <sup>b</sup>	6.12 ± 0.38 µg/mL <sup>b</sup>
<b>SP extract</b>	49.34 ± 2.72 µg/mL <sup>c</sup>	39.83 ± 2.59 µg/mL <sup>c</sup>

**Notes:** IC<sub>50</sub>, concentration of drug needed to inhibit cell viability by 50%. Values are means + SD of triplicate experiments. Means in the same column with different letters were significantly different (P<0.05), ANOVA, Tukey-HSD. Means in the same column with different letters were significantly different (P < 0.05).

potency. IC<sub>50</sub> values of cancer cells treated with AuNPs, CuNPs and SP extract are given in Table 4. Table 4 shows that IC<sub>50</sub> values of AuNPs and CuNPs against MCF-7 and MDA-MB-231 cell lines were lower than those of SP. This is a strong evidence that both AuNPs and CuNPs have higher anticancer effect than that of SP against the breast cancer cells studied. It can also be seen that CuNPs have better anticancer activity (have lower IC<sub>50</sub> values) than AuNPs against MCF-7 and MDA-MB-231 cell lines. The CuNPs showed significantly higher p values when compared to AuNPs and showed potent activity against MCF-7 cell line (IC<sub>50</sub> of 19.34 ± 1.68 µg/mL) and against MDA-MB-231 cell line (IC<sub>50</sub> of 6.12 ± 0.38 µg/mL), while the p values of AuNPs were higher than SP extract and showed effectiveness against for MCF-7 cell line (IC<sub>50</sub> value 42.41 ± 2.63 µg/mL) and against MDA-MB-231 cell line (IC<sub>50</sub> value 23.73 ± 1.75 µg/mL). These results showed that the toxic effect of the studied substances was higher on MDA-MB-231 cells than on MCF-7 cells. In a previous study, the toxic effect of zinc oxide nanoparticles synthesized from the aqueous extract of SP wood was evaluated against HT-29 cancer cell line using the MTT method.<sup>19</sup> It was found that these NPs showed high anticancer activity and IC<sub>50</sub> was 262.78 µg/mL. IC<sub>50</sub> was 19.77 ± 0.98 µg/mL on MCF-7 for CuNPs of *Tamarindus indica*.<sup>52</sup> The improved activity of nanoparticles over those of plant extracts were observed in more than one previous study.<sup>12</sup> For example, green AuNPs synthesized from the aqueous extract of *Hygrophila spinosa* were found to be more active than the plant extract in vitro against MCF-7 and MDA-MB-231.<sup>12</sup> The authors suggested that this effect may be due to the increased cellular uptake and retention of the NPs. Physicochemical properties of the nanoparticles such as size, shape, composition, nature of the capping agent, and coating may influence uptake of NPs by cells are therefore involved in the toxicity of the nanoparticles.<sup>12,54</sup> For example, it was found that triangular-shaped nanomaterials exhibit greater toxic potency relative to spherical NPs and that spherical NPs undergo the fastest internalization followed by cubic, rod-shaped and disk-like NPs.<sup>55</sup> This may explain the great toxicity of CuNPs in relation to AuNPs in our work, as the CuNPs were more spherical. Nanoparticles penetrate into mammalian cells by phagocytosis or endocytosis.<sup>55</sup> The NPs tend to release metal ions into the cell with an increase in the formation of reactive oxygen species (ROS), which leads DNA destruction and mitochondrial membrane potential disorder and to the activation of programmed death of cancer cells.<sup>55</sup>

## The Binding Affinity of Selected SP Compounds into 5,10-Methenyltetrahydrofolate Synthetase Receptor Docking Studies

To understand the molecular interactions of the major phytochemical compounds from SP against breast cancer cells, molecular docking studies were carried out with cancer target methenyl tetrahydrofolate synthetase (MTHFS) (Protein Data Bank ID: 3HY3).<sup>27</sup> MTHFS expression enhances folate-dependent de novo purine biosynthesis, which is an essential component for the growth and proliferation of cells. MTHFS is increased in tumors and inhibition of MTHFS in human MCF-7 breast cancer cells has been shown to arrest the growth of cells.<sup>56</sup> Each of the selected phytochemical compounds and co-crystallized ligand, 10F, was docked into active site of MTHFS. The binding affinities were evaluated on the basis of the binding free energy S-score, hydrogen bonds with the distance between the selected phytochemical compounds (the root-mean-square deviation of atomic positions (RMSD) and the amino acid residues in the receptor of MTHFS (Table 5).

Compounds which gave the best docking score based on the binding free energy, H-bonding, distance with the amino acid residue in the receptor and RMSD from the native ligand were beta-sitosterol, 3-beta-hydroxylean, 7-methyl-Z-tetradecen and stigmast-5-ene, 3-beta-(trimethylsilyl) with S-scores of -12.00, -11.88, -11.18 and -11.01 kcal/mol, respectively. As expected, these compounds bind to the ATP site in a positively charged cleft region between strand β6

**Table 5** Summary of Molecular Docking Results for the Phytochemical Compounds of SP with the MTHFS

Phytochemical Ligands	Hydrogen Bonds Between Atoms of Ligands and Amino Acids of Receptor					S-Score (Binding Energy) (kcal/mol)
	Ligands Atoms	Receptor		Type	Distance (Å)	
		Atoms	Residues			
10F	H 3073	O 853	LEU 56	H-donor	1.71	-15.95
	H 3074	OE 930	GLU 61	H-donor	2.90	
	H 3077	OE 931	GLU 61	H-donor	1.89	
	O 3080	OH 2352	TYR 152	H-donor	2.89	
	H 3085	OH 2352	TYR 152	H-donor	2.18	
	O 3080	NE 2300	ARG 148	H-acc	2.96	
	O 3080	OH 2352	TYR 152	H-acc	2.89	
3.beta-hydroxylean	O 3130	OH 2373	TYR 153	H-acc	2.98	-11.88
	H 3112	O 853	LEU 56	H-don	2.22	
7-methyl-Z- tetradecen	O 3072	N 848	LEU 56	H-acc	2.83	-11.18
Beta -Sitosterol	H 3127	O 2290	ARG 148	H-don	3.49	-12.00
	O 3126	OH 2373	TYR 153	H-don	2.64	
	O 3126	OH 2373	TYR 153	H-acc	2.64	
Stigmast-5-ene, 3.beta.-(trimethylsiloxy)-, (24S)-	C 3092	OH 2352	TYR 152	H-acc	9.74	-11.01
Phenol 2,4 phosphite	C 3073	OH 2352	TYR 152	H-acc	3.83	-10.28

and helix  $\alpha 5$ . The short helix ( $\alpha 4$ ) and a long loop inserted between strands  $\beta 3$  and  $\beta 4$  act like a cap and are seen partially covering the active site. The extracted compounds had bound with Tyr 152, and Tyr 151 residue of MTHFS receptor in the middle of the channel connecting ATP binding site with the substrate-binding pocket, precluding the positioning of gamma-phosphate for a nucleophilic attack, owing to steric hindrance.

All the docked ligands also exhibited similar interactions as mentioned earlier concerning co-crystal ligand (10 F) (Figure 8A and B). A total of 13 residues were found at the binding of the human MTHFS—10F complex while 19 residues were seen in the human MTHFS—3.beta-hydroxylean complex. In addition, a total number of 17 residues were shown in the human MTHFS—7-methyl-Z- tetradecen, 13 residues were shown in the human MTHFS—phenol 2.4 phosphite, and 10 residues were shown in the human MTHFS—Beta—Sitosterol. Finally, a total number of 8 residues were shown in the human MTHFS—Stigmast (Figure 8B). Interestingly, selected compounds phenol 2.4 phosphite, 3.beta-hydroxylean, Beta—Sitosterol, and Stigmast-5-ene, 3.beta.-(trimethylsiloxy) are observed to adopt a conformation close to a coplanar cis-diaryldiazine. The energetically less-favorable cis ligand conformation, compared to the trans arrangement, appears to be preferred because it enables simultaneous interaction with the aromatic moieties. The twisting of the aromatic ring probably helps bring the reacting functional groups in close proximity and adjust their orientation. The glutamate protrudes out of the binding pocket through a circular hole at the top and is lying on the surface of the protein. Numerous hydrophobic van der Waals contacts are observed between the aromatic ring and the aromatic side. Thus, from the data, the compounds which gave the best docking score based on the binding free energy and H-bonding with it distance between the amino acid in the receptor and RMSD from the native ligand were beta —Sitosterol, 3.beta-hydroxylean, and 7-methyl-Z- tetradecen with S-score -12.00, -11.88, and -11.18 kcal/mol, respectively (Table 5).

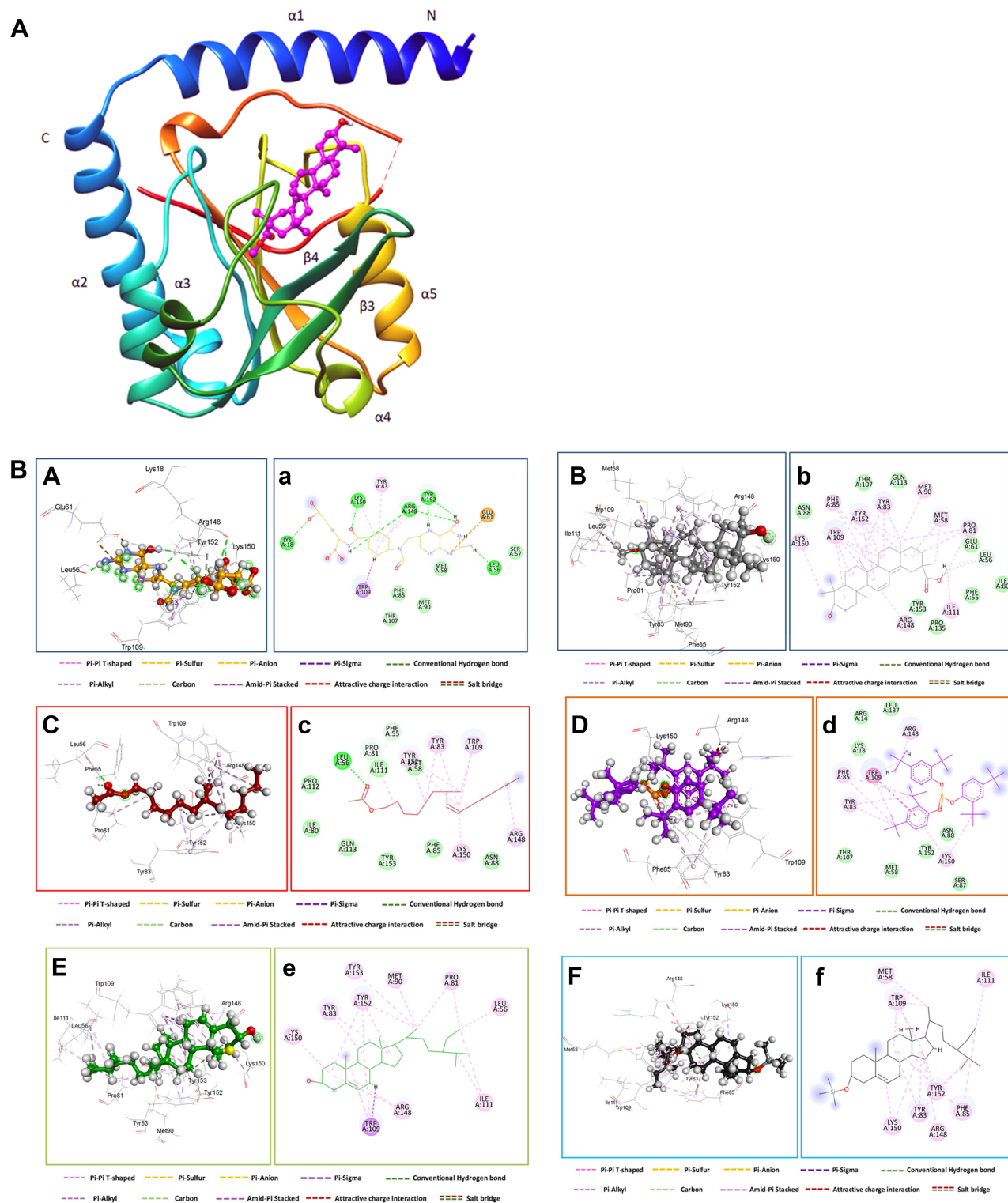


**Figure 8** (A) Three-dimensional crystal structure of 3.β-hydroxylean within the catalytic binding site of the MTHFS (Protein Data Bank ID: 3HY3). (B) Molecular docking analysis for the bioactive compound of SE and co-crystallized ligand (10F) and their interaction with amino acid residues at the active site of MTHFS. Three-dimensional (capital letter) and second-dimensional Interactions (small letter) of (A) co-crystallized ligand (10F), (B) 3.β-hydroxylean, (C) 7-methyl-Z-tetradecen, (D) phenol 2,4 phosphite, (E) Beta-Sitosterol, (F) Stigmast-5-ene, 3.β-(trimethylsiloxy) and binding sites with MTHFS.

## Conclusion

In this study, green AuNPs and CuNPs were synthesized via a rapid, simple, inexpensive, and environmentally friendly approach using the fruit extract of SP. The various biomolecules present in the fruit extract of SP were used as reducing, stabilizing, and capping agents for the NPs. The bio fabricated of NPs were characterized by UV–Vis spectroscopy, FT-IR, TEM, EDX, and Zeta sizer analysis. Antioxidant and anticancer properties of AuNPs and CuNPs synthesized in green media were performed and showed dose-dependent activity. Both Au and Cu NPs showed significant cytotoxicity against MCF-7 and MDA-MB-231 cancer cells. Moreover, both Au and CuNPs have promising antibacterial effects against pathogenic bacterial strains. Green synthesized NPs exhibited enhanced biological activity compared to SP extract. Overall, this green synthesized AuNPs and CuNPs from fruit extract of SP have the potential for their use in the pharmaceutical and biomedical fields. Despite their excellent performance in improving anticancer and antioxidant activity, further research into the detailed toxicity profiles and metabolic mechanisms of Au and CuNPs is still needed.

## Acknowledgments

The authors would like to thank UAE research office for financial assistance to cover the publication fees of this article. We are also indebted to Dr. Mohamed El Olama from Zayed Complex for Herbal for collecting the SP plant fruits.

## Disclosure

The authors report no conflicts of interest in this work.

## References

1. Jahan I, Erci F, Isildak I. Facile microwave-mediated green synthesis of non-toxic copper nanoparticles using Citrus sinensis aqueous fruit extract and their antibacterial potentials. *J Drug Deliv Sci Technol.* 2021;61:102172. doi:10.1016/j.jddst.2020.102172
2. Saravanan A, Kumar PS, Karishma S, et al. A review on biosynthesis of metal nanoparticles and its environmental applications. *Chemosphere.* 2021;264:128580. doi:10.1016/j.chemosphere.2020.128580
3. Soni V, Raizada P, Singh P, et al. Sustainable and green trends in using plant extracts for the synthesis of biogenic metal nanoparticles toward environmental and pharmaceutical advances: a review. *Environ Res.* 2021;202:111622. doi:10.1016/j.envres.2021.111622
4. Hasanin M, Al Abboud MA, Alawlaqi MM, et al. Ecofriendly synthesis of biosynthesized copper nanoparticles with starch-based nanocomposite: antimicrobial, antioxidant, and anticancer activities. *Biol Trace Elem Res.* 2022;200:2099–2112. doi:10.1007/s12011-021-02812-0
5. de Jesus RA, de Assis GC, de Oliveira RJ, et al. Environmental remediation potentialities of metal and metal oxide nanoparticles: mechanistic biosynthesis, influencing factors, and application standpoint. *Environ Technol Innov.* 2021;24:101851. doi:10.1016/j.eti.2021.101851
6. John MS, Nagoth JA, Zannotti M, et al. Biogenic synthesis of copper nanoparticles using bacterial strains isolated from an Antarctic consortium associated to a psychrophilic marine ciliate: characterization and potential application as antimicrobial agents. *Mar Drugs.* 2021;19:263.
7. Salem SS, Badawy MSE, Al-Askar AA, et al. Green biosynthesis of selenium nanoparticles using Orange peel waste: characterization, antibacterial and antibiofilm activities against multidrug-resistant bacteria. *Life.* 2022;12:893.
8. Hasanin M, Hashem AH, Lashin I, et al. In vitro improvement and rooting of banana plantlets using antifungal nanocomposite based on mycosynthesized copper oxide nanoparticles and starch. *Biomass Convers Biorefin.* 2021;6:1–11.
9. Hashem AH, Salem SS. Green and ecofriendly biosynthesis of selenium nanoparticles using Urtica dioica (stinging nettle) leaf extract: antimicrobial and anticancer activity. *Biotechnol J.* 2022;17:2100432.
10. Mittal AK, Chisti Y, Banerjee UC. Synthesis of metallic nanoparticles using plant extracts. *Biotechnol Adv.* 2013;31:346–356. doi:10.1016/j.biotechadv.2013.01.003
11. Jadoun S, Verma A, Arif R. Green synthesis of nanomaterials for textile applications. In: *Green Chemistry for Sustainable Textiles.* Elsevier; 2021:315–324.
12. Letchumanan D, Sok SP, Ibrahim S, et al. Plant-based biosynthesis of copper/copper oxide nanoparticles: an update on their applications in biomedicine, mechanisms, and toxicity. *Biomolecules.* 2021;11:564. doi:10.3390/biom11040564
13. Siddiqi KS, Husen A. Recent advances in plant-mediated engineered gold nanoparticles and their application in biological system. *J Trace Elem Med Biol.* 2017;40:10–23. doi:10.1016/j.jtemb.2016.11.012
14. Al Bratty M, Makeen HA, Alhazmi HA, et al. Phytochemical, cytotoxic, and antimicrobial evaluation of the fruits of miswak plant, *Salvadora persica* L. *J Chem.* 2020;2020:29.
15. Tatke P, Nehete M, Gabhe S. Antioxidant, antimicrobial and wound healing activity of *Salvadora persica* twig extracts. *J Complement Med Altern Healthc.* 2018;7:555720.
16. Al-Dabbagh B, Elhaty IA, Murali C, et al. *Salvadora persica* (Miswak): antioxidant and promising antiangiogenic insights. *Am J Plant Sci.* 2018;9:1228. doi:10.4236/ajps.2018.96091
17. Varijakzhan D, Chong C-M, Abushelaibi A, et al. Middle Eastern plant extracts: an alternative to modern medicine problems. *Molecules.* 2020;25(5):1126. doi:10.3390/molecules25051126
18. Jiang X, He C, Lin W. Supramolecular metal-based nanoparticles for drug delivery and cancer therapy. *Curr Opin Chem Biol.* 2021;61:143–153. doi:10.1016/j.cbpa.2021.01.005



19. Miri A, Sarani M. Biosynthesis and cytotoxic study of synthesized zinc oxide nanoparticles using *Salvadora persica*. *BioNanoScience*. 2019;9:164–171. doi:10.1007/s12668-018-0579-3
20. Arshad H, Sami MA, Sadaf S, et al. *Salvadora persica* mediated synthesis of silver nanoparticles and their antimicrobial efficacy. *Sci Rep*. 2021;11:1–11. doi:10.1038/s41598-021-85584-w
21. Hamza AA, Khasawneh MA, Elwy HM, et al. *Salvadora persica* attenuates DMBA-induced mammary cancer through downregulation oxidative stress, estrogen receptor expression and proliferation and augmenting apoptosis. *Biomed Pharmacother*. 2022;147:112666. doi:10.1016/j.biopha.2022.112666
22. Abdelmonem R, Elhabal SF, Abdelmalak NS, et al. Formulation and characterization of Acetazolamide/carvedilol niosomal gel for glaucoma treatment: in vitro, and in vivo study. *Pharmaceutics*. 2021;13:221. doi:10.3390/pharmaceutics13020221
23. Johnson J, Mani J, Ashwath N, et al. Potential for Fourier transform infrared (FTIR) spectroscopy toward predicting antioxidant and phenolic contents in powdered plant matrices. *Mol Biomol Spectrochim*. 2020;233:118228. doi:10.1016/j.saa.2020.118228
24. Jagwani D, Krishna PH. Nature's nano-assets: green synthesis, characterization techniques and applications—A graphical review. *Mater Today Proc*. 2021;46:2307–2317.
25. Nenadis N, Lazaridou O, Tsimidou MZ. Use of reference compounds in antioxidant activity assessment. *J Agric Food Chem*. 2007;55:5452–5460. doi:10.1021/jf070473q
26. Sylvester PW. Optimization of the tetrazolium dye (MTT) colorimetric assay for cellular growth and viability. In: *Drug Design and Discovery*. Springer; 2011:157–168.
27. Wu D, Li Y, Song G, et al. Structural basis for the inhibition of human 5, 10-methylenetetrahydrofolate synthetase by N10-substituted folate analogues. *Cancer Res*. 2009;69:7294–7301. doi:10.1158/0008-5472.CAN-09-1927
28. Elgorban AM, Bahkali AH, Al Farraj DA, et al. Natural products of *Alternaria* sp., an endophytic fungus isolated from *Salvadora persica* from Saudi Arabia. *Saudi J Biol Sci*. 2019;26:1068–1077. doi:10.1016/j.sjbs.2018.04.010
29. Mohamad OA, Li L, Ma J-B, et al. Evaluation of the antimicrobial activity of endophytic bacterial populations from Chinese traditional medicinal plant licorice and characterization of the bioactive secondary metabolites produced by *Bacillus atrophaeus* against *Verticillium dahliae*. *Front Microbiol*. 2018;9:924. doi:10.3389/fmicb.2018.00924
30. Paritala V, Chiruvella KK, Thammineni C, et al. Phytochemicals and antimicrobial potentials of mahogany family. *Revista Brasileira de Farmacognosia*. 2015;25:61–83.
31. Tu J, Sun HX, Ye YP. 3 $\beta$ -hydroxyolean-12-en-27-oic acid: a cytotoxic, apoptosis-inducing natural drug against COLO-205 cancer cells. *Chem Biodivers*. 2006;3:69–78. doi:10.1002/cbdv.200690009
32. Ullah H, Khan H. Epigenetic drug development for autoimmune and inflammatory diseases. In: *Histone Modifications in Therapy*. Elsevier; 2020:395–413.
33. Zhao F, Wang P, Lucardi RD, et al. Natural sources and bioactivities of 2, 4-di-tert-butylphenol and its analogs. *Toxins*. 2020;12:35. doi:10.3390/toxins12010035
34. Sun H-X, Zheng Q-F TJ. Induction of apoptosis in HeLa cells by 3 $\beta$ -hydroxy-12-oleanen-27-oic acid from the rhizomes of *Astilbe chinensis*. *Bioorg Med Chem*. 2006;14:1189–1198. doi:10.1016/j.bmc.2005.09.043
35. Idan SA, Al-Marzoqi AH, Hameed IH. Spectral analysis and anti-bacterial activity of methanolic fruit extract of *Citrullus colocynthis* using gas chromatography-mass spectrometry. *Afr J Biotechnol*. 2015;14:3131–3158. doi:10.5897/AJB2015.14957
36. Liu Q, Wu F, Chen Y, et al. Anti-human colon cancer properties of a novel chemotherapeutic supplement formulated by gold nanoparticles containing *Allium sativum* L. leaf aqueous extract and investigation of its cytotoxicity and antioxidant activities. *Arab J Chem*. 2021;14:103039. doi:10.1016/j.arabjc.2021.103039
37. Ahn E-Y, Lee YJ, Park J, et al. Antioxidant potential of *Artemisia capillaris*, *Portulaca oleracea*, and *Prunella vulgaris* extracts for biofabrication of gold nanoparticles and cytotoxicity assessment. *Nanoscale Res Lett*. 2018;13:1–14. doi:10.1186/s11671-018-2751-7
38. Shah AA, Jayalakshmi D, Xavier B. Characterization of gold nanoparticles synthesized from *Solanum torvum* (Turkey Berry) fruit extract and its application in catalytic degradation of methylene blue and antibacterial properties. *Mater Today Proc*. 2021;47:927–932.
39. Satpathy S, Patra A, Ahirwar B, et al. Process optimization for green synthesis of gold nanoparticles mediated by extract of *Hygrophila spinosa* T. Anders and their biological applications. *Physica E*. 2020;121:113830. doi:10.1016/j.physe.2019.113830
40. Sk I, Khan MA, Haque A, et al. Synthesis of gold and silver nanoparticles using *Malva verticillata* leaves extract: study of gold nanoparticles catalysed reduction of nitro-Schiff bases and antibacterial activities of silver nanoparticles. *Curr Opin Green Sustain Chem*. 2020;3:100006. doi:10.1016/j.crgsc.2020.05.003
41. Divakaran D, Lakkakula JR, Thakur M, et al. Dragon fruit extract capped gold nanoparticles: synthesis and their differential cytotoxicity effect on breast cancer cells. *Mater Lett*. 2019;236:498–502. doi:10.1016/j.matlet.2018.10.156
42. Rajeshkumar S, Menon S, Kumar SV, et al. Antibacterial and antioxidant potential of biosynthesized copper nanoparticles mediated through *Cissampelos amotiana* plant extract. *J Photochem Photobiol B*. 2019;197:111531. doi:10.1016/j.jphotobiol.2019.111531
43. Al-Khafaji MAA, Al-Refai'a RA, Al-Zamely OMY. Green synthesis of copper nanoparticles using *Artemisia* plant extract. *Mater Today Proc*. 2022;49:2831–2835.
44. Ginting B, Maulana I, Karnila I. Biosynthesis copper nanoparticles using *Blumea balsamifera* leaf extracts: characterization of its antioxidant and cytotoxicity activities. *Surf Interfaces*. 2020;21:100799. doi:10.1016/j.surf.2020.100799
45. Nagar N, Devra V. Green synthesis and characterization of copper nanoparticles using *Azadirachta indica* leaves. *Mater Chem Phys*. 2018;213:44–51. doi:10.1016/j.matchemphys.2018.04.007
46. Singh RK, Srivastava P, Prakash O. Biosynthesis of gold nanoparticles using leaf extract of *Salvadora persica* and its role in boosting urease performance via immobilization. *J Plant Biochem Biotechnol*. 2021;30:623–628. doi:10.1007/s13562-021-00649-1
47. Hosny M, Fawzy M. Instantaneous phytosynthesis of gold nanoparticles via *Persicaria salicifolia* leaf extract, and their medical applications. *Adv Powder Technol*. 2021;32:2891–2904. doi:10.1016/j.apt.2021.06.004
48. Sasidharan D, Namitha T, Johnson SP, et al. Synthesis of silver and copper oxide nanoparticles using *Myristica fragrans* fruit extract: antimicrobial and catalytic applications. *Sustain Chem Pharm*. 2020;16:100255. doi:10.1016/j.sep.2020.100255
49. Sizochenko N, Mikolajczyk A, Syzochenko M, et al. Zeta potentials ( $\zeta$ ) of metal oxide nanoparticles: a meta-analysis of experimental data and a predictive neural networks modeling. *NanoImpact*. 2021;22:100317. doi:10.1016/j.impact.2021.100317

50. Pisoschi AM, Pop A. The role of antioxidants in the chemistry of oxidative stress: a review. *Eur J Med Chem.* 2015;97:55–74. doi:10.1016/j.ejmech.2015.04.040
51. Aghamirzaei M, Khiabani MS, Hamishehkar H, et al. Antioxidant, antimicrobial and cytotoxic activities of biosynthesized gold nanoparticles (AuNPs) from Chinese lettuce (CL) leave extract (*Brassica rapa* var. *pekinensis*). *Mater Today Commun.* 2021;29:102831. doi:10.1016/j.mtcomm.2021.102831
52. Rehana D, Mahendiran D, Kumar RS, et al. Evaluation of antioxidant and anticancer activity of copper oxide nanoparticles synthesized using medicinally important plant extracts. *Biomed Pharmacother.* 2017;89:1067–1077.
53. Abbas AH, Fairouz NY. Characterization, biosynthesis of copper nanoparticles using ginger roots extract and investigation of its antibacterial activity. *Mater Today.* 2021;61:908.
54. Medici S, Peana M, Pelucelli A, et al. An updated overview on metal nanoparticles toxicity. In: *Seminars in Cancer Biology*. Elsevier; 2021.
55. Vaid P, Raizada P, Saini AK, et al. Biogenic silver, gold and copper nanoparticles-A sustainable green chemistry approach for cancer therapy. *Sustain Chem Pharm.* 2020;16:100247.
56. Field MS, Anguera MC, Page R, et al. 5, 10-Methenyltetrahydrofolate synthetase activity is increased in tumors and modifies the efficacy of antipurine LY309887. *Arch Biochem Biophys.* 2009;481:145–150.

International Journal of Nanomedicine

Dovepress

## Publish your work in this journal

The International Journal of Nanomedicine is an international, peer-reviewed journal focusing on the application of nanotechnology in diagnostics, therapeutics, and drug delivery systems throughout the biomedical field. This journal is indexed on PubMed Central, MedLine, CAS, SciSearch®, Current Contents®/Clinical Medicine, Journal Citation Reports/Science Edition, EMBase, Scopus and the Elsevier Bibliographic databases. The manuscript management system is completely online and includes a very quick and fair peer-review system, which is all easy to use. Visit <http://www.dovepress.com/testimonials.php> to read real quotes from published authors.

Submit your manuscript here: <https://www.dovepress.com/international-journal-of-nanomedicine-journal>